A Straightforward Route to Copper/Zinc Oxide Nanocomposites: The Controlled Thermolysis of $Zn[Cu(CN)_3]$

Yanzhi Guo,[a] Rainer Weiss,[a] and Matthias Epple*[a]

Keywords: Cyanides / Copper / Zinc / Thermochemistry / EXAFS spectroscopy

Copper–zinc nanocomposites were prepared by thermolysis of copper–zinc cyanides under mild conditions. Two different routes were used for the preparation of the cyanide complex: A batch precipitation method and the continuous overflow precipitation method. The thermolysis of the cyanides was studied in-situ by thermogravimetry coupled with infrared spectroscopy (TG-IR) and by thermogravimetry coupled with mass spectroscopy (TG-MS). The structure of the nanocomposites was investigated by X-ray powder diffraction (XRD) and extended X-ray absorption fine structure (EXAFS). Geometric models were suggested on the atomic scale based on EXAFS results for the precursor, the mixed oxides (CuO/ZnO), and the reduced copper–zinc samples (Cu/ZnO, i.e. catalyst for methanol synthesis). In the batch precipitation method, the influence of temperature on the morphology of the thermolysis products was explored. In the continuous overflow method, the morphology of the Cu–Zn cyanide complex was investigated as a function of concentration and residence time. A high solution concentration and a short residence time (equivalent to a high flow rate) led to smaller particles.

Introduction

Copper–zinc oxide nanocomposites can be obtained in a variety of morphologies, including thin films,[1] nanowires[2] and nanoparticles.[3] High surface area copper/zinc oxide is an active catalyst for methanol synthesis, for water-gas shift reactions, and for various hydrogenations.[4] It is widely accepted that zinc oxide can improve the dispersion of copper and thereby the catalytic activities.[5] Copper–zinc oxide nanocomposites are usually prepared by co-precipitation from aqueous solutions. Typically, a mixed solution of copper and zinc salts (usually nitrates or acetates) is prepared and the precipitation of both carbonates is induced by addition of sodium or ammonium carbonate whilst stirring, followed by drying and calcination.[6–9] The particle size and crystallinity of the products can be adjusted by the pH, the concentration, the stirring rate, the duration of precipitation and aging, and the calcination conditions.[10] Pollard et al.[4] used the minerals georgeite $[Cu_5(CO_3)_3(OH)_4{\cdot}6H_2O]$ and azurite $[Cu_3(CO_3)_2(OH)_2]$ as precursors for copper–zinc mixed oxides. Recently, a nonaqueous organometallic route was developed by Hambrock et al.[11] and uniform copper–zinc nanoparticles were obtained. They used $Cu[OCH(Me)CH_2NMe_2]$ and Et_2Zn as precursors. The thermolysis was carried out in the coordinating solvent hexadecylamine at elevated temperatures and nano-scale colloidal copper–zinc systems with different zinc contents were obtained. Zhou et al.[2] prepared copper–zinc nanowires by heating CuI_2 and ZnI_2 in a dynamic oxygen atmosphere. A self-catalysed vapour-liquid-solid growth mechanism was suggested.

Polymeric metal cyanides represent a homogeneous mixture of the individual metals on the atomic length scale. The heterogeneous mixing of individual compounds is therefore avoided. The controlled thermolysis of these compounds can be carried out at comparatively low temperature due to the presence of a suitable organic leaving group, i.e. the cyanide in the precursors. A higher temperature is usually required in conventional syntheses to achieve a sufficiently fast diffusion. We have shown that the composition as well as the crystal structure of the bimetallic Fe–Sn and Ru–Sn composites can be fine-tuned by the thermolysis conditions such as time, temperature and the atmosphere.[12–14] Such systems are suitable precursors for the preparation of bimetallic nanocomposites that incorporate the initially blended metals.

Recently we adopted the continuous overflow method for the preparation of calcium phosphate nanoparticles from solution.[15] The particle size, morphology and crystallinity can be adjusted by the process parameters, mainly the residence time (the flow rate of the solutions), and the concentration of the solutions. It was therefore the aim of this work to prepare a suitable cyanide precursor for the Cu/ZnO system and to control its morphology by different crystallisation methods. Thereby, the properties of the final product should be adjustable.[16–18]

[a] Inorganic Chemistry, University of Duisburg-Essen, Universitätsstr. 5–7, 45117 Essen, Germany
Fax: +49-201-183-2621
E-mail: matthias.epple@uni-due.de

Result and Discussion

For the preparation of the Cu–Zn cyanide complex, there are two possible routes as shown in Equations (1), (2) and (3). In both cases, tetrahedral $[Zn(CN)_4]^{2-}$ is formed in the first step (1). Subsequently, both reactions (2) and (3) are likely to occur. Because the stability constant of $[Zn(CN)_4]^{2-}$ (4×10^{19} M^{-4})[19] is smaller than that of $[Cu(CN)_4]^{2-}$ (1×10^{27} M^{-4}),[20] the latter compound is preferred in equilibrium. However, the oxidation state of $[Cu(CN)_4]^{2-}$ is not stable leading to a reduction of Cu^{II} to Cu^{I}. Thus, a transient state of $[Cu(CN)_3]^{2-}$ can be assumed, followed by the formation of $Zn[Cu(CN)_3]$ as precipitate and the release of $(CN)_2$ into the gas phase.

$$4\ CN^- + Zn^{2+} \rightarrow [Zn(CN)_4]^{2-} \quad (1)$$

$$[Zn(CN)_4]^{2-} + Cu^{2+} \rightarrow Cu[Zn(CN)_4]\ \downarrow \quad (2)$$

$$[Zn(CN)_4]^{2-} + Cu^{2+} \rightarrow Zn[Cu(CN)_4] \rightarrow Zn[Cu(CN)_3]\downarrow + \tfrac{1}{2}\ (CN)_2\ \uparrow \quad (3)$$

Batch-Wise Preparation and Thermolysis

For the Cu–Zn cyanide complex prepared by the batch precipitation method, elemental analysis gave 17.5 wt.-% C, 20.2 wt.-% N, 30.3 wt.-% Cu and 31.2 wt.-% Zn. This corresponds to a Cu/Zn/CN molar ratio of 1:1:3.1. We conclude that $Zn[Cu(CN)_3]$ (calcd. 17.4 wt.-% C, 20.3 wt.-% N, 30.7 wt.-% Cu and 31.6 wt.-% Zn) is the main component of the precipitates and a small amount of $Cu[Zn(CN)_4]$ (calcd. 20.6 wt.-% C, 24.0 wt.-% N, 27.3 wt.-% Cu and 28.1 wt.-% Zn) is also present. The infrared spectra of this complex support this assumption (Figure 1). The strong peak at 2155 cm^{-1} is the contribution of CN groups bound (via carbon) to Cu^{I}.[21] An additional contribution at 2217 cm^{-1} is attributed to CN bound (via carbon) to Zn.[22] It is obvious that $Zn[Cu(CN)_3]$ is dominating in the prepared cyanides due to its high peak intensity in the spectra.

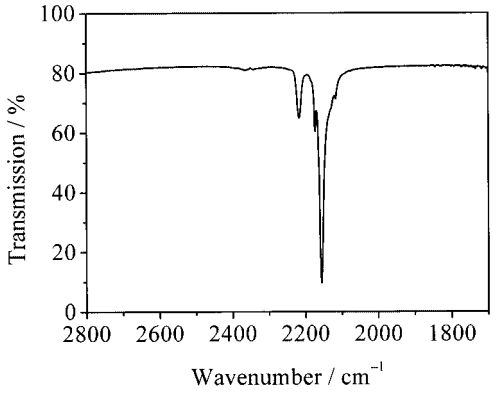

Figure 1. Infrared spectra of $Zn[Cu(CN)_3]$, prepared by the batch precipitation method.

The thermolysis of the copper–zinc complex was studied by thermogravimetric analysis coupled with infrared spectroscopy (TG-IR). When heated up under oxygen, the decomposition of the copper–zinc complex started at about 300 °C (Figure 2, part a). Two steps at about 440 °C and 510 °C can be derived from the TG weight loss curve. The weight loss ceased at about 530 °C. At 1000 °C, only CuO/ZnO was present, as shown by XRD. The total weight loss was about 23%. From the weight loss it can be deduced that the precursor consists of $Zn[Cu(CN)_3]$ (a theoretical weight loss of 22.2% for a complete transformation to CuO/ZnO) rather than $Cu[Zn(CN)_4]$ (a theoretical weight loss of 30.9%). This is in good agreement with the elemental analysis. Two exothermal peaks in the DTA curve correspond to the two steps in the weight loss curve, indicating oxidative combustion.

The infrared spectra in Figure 2 (part b) correspond to the evolved gas phase during heating. The contribution of

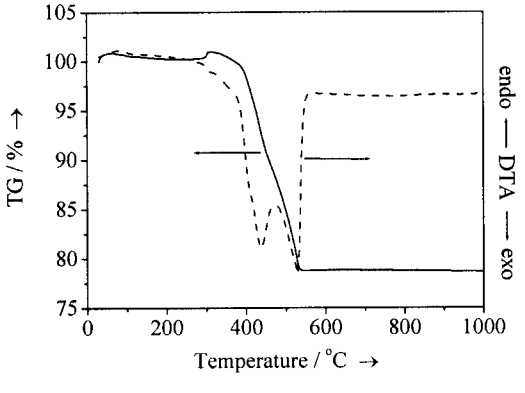

(a)

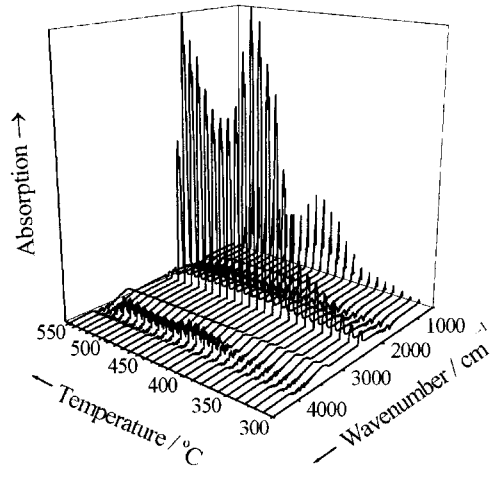

(b)

Figure 2. Thermogravimetric analysis of $Zn[Cu(CN)_3]$ under oxygen (a) and the corresponding time-resolved infrared spectra of the released gases during heating (b) (heating rate 5 K min^{-1}).

cyanides (CN, at 2343 cm^{-1}) appeared first. Carbon dioxide (C=O, 2360/2312/671 cm^{-1}) was subsequently released at elevated temperature, showing again the two steps at about 440 °C and 510 °C, indicated by the two maxima in the time-resolved spectra.

Another experiment was carried out with thermogravimetric analysis coupled with mass spectroscopy (TG-MS). Air was used as oxidizing gas and the copper–zinc complex was heated from room temperature to 1000 °C. The weight loss started at about 300 °C and stopped at around 620 °C (Figure 3, part a). The thermolysis was shifted to higher temperature compared with the TG-IR results because oxygen was replaced by air and the heating rate was increased from 5 K min^{-1} to 10 K min^{-1}. The total weight loss was

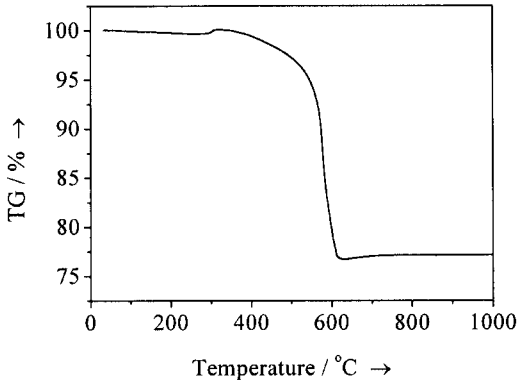

(a)

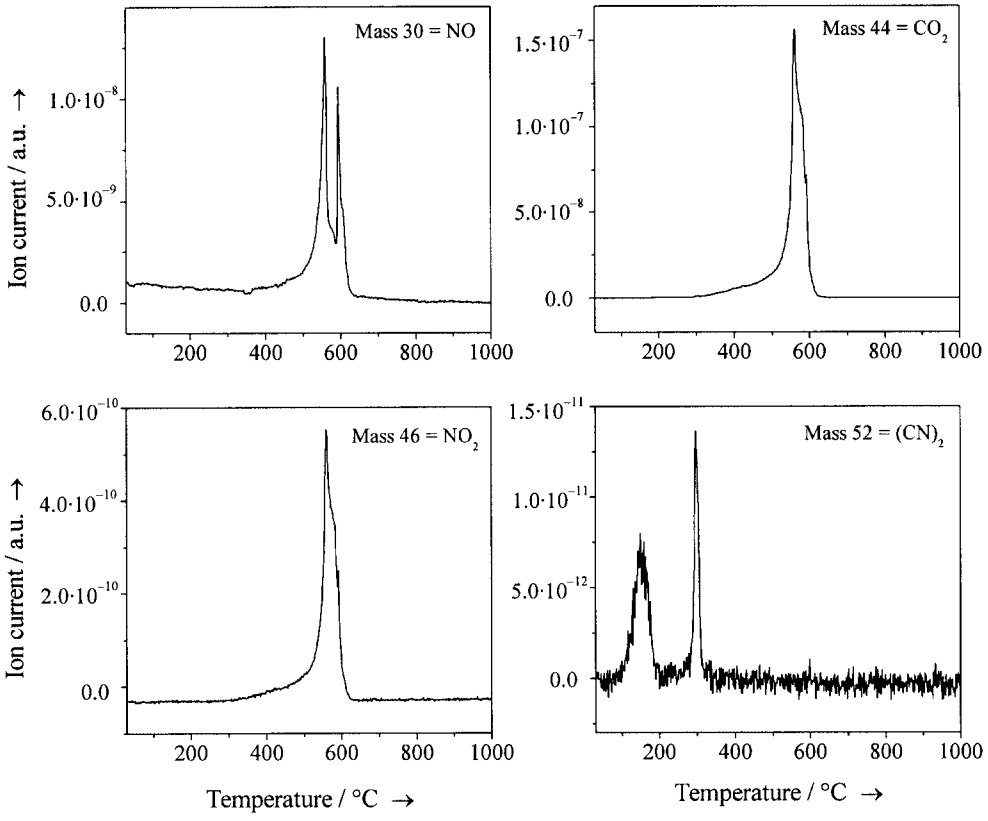

(b)

Figure 3. (a) Thermogravimetric analysis of $Zn[Cu(CN)_3]$ under air, (b) the corresponding time-resolved mass spectra of four different masses in the released gases (heating rate 10 K min^{-1}).

about 24 wt.-%. The mass spectra in Figure 3 (part b) clearly show the release of gaseous species. Cyanogen [$(CN)_2$: mass 52] was released at low temperatures in two steps, corresponding to the low intensity of the cyanide peak in the IR spectra. The initial "dip" in the TG curve at around 300 °C can be related to a non-oxidative elimination of cyanogen. The release of carbon dioxide, nitrogen monoxide and nitrogen dioxide at higher temperatures occurred in two steps, indicated by two peaks or a broad peak with a shoulder.

The XRD patterns of the thermolysis products under air at different temperatures are shown in Figure 4, part a. Copper oxide and zinc oxide are present. With rising thermolysis temperature, the height of the peaks increased and their width decreased, indicating an increasing particle size (a better crystallinity). The three oxides samples of Figure 4, (part a) were then reduced at 250 °C in H_2/N_2 to Cu/ZnO. The effects of the initial thermolysis temperatures under air are also represented in the XRD patterns of the reduced samples (Figure 4, part b).

EXAFS analysis was performed to investigate the crystal structure of the copper zinc cyanide complex (no single crystals could be obtained so far), of the oxide mixtures (CuO/ZnO), and of the reduced samples (Cu/ZnO). Figure 5 (part a) shows the Cu *K*-edge EXAFS Fourier transform magnitudes (FTs) of the complex $Zn[Cu(CN)_3]$. The nearest neighbours derived from the FTs were fit as 3 carbon atoms at 1.92 Å (Table 1, part a). Another carbon atom appeared at a larger distance, at 2.37 Å. This can be ascribed to different Cu–CN bonds.[21] In this case the coordination polyhedron around Cu can be described as deformed trigonal pyramid with one CN group at a larger distance. The corresponding nitrogen atoms in cyanide appear at 3.12 Å (3 N) and 3.71 Å (1 N), respectively. The Zn *K*-edge EXAFS Fourier transform magnitude of the complex is shown in Figure 5, part b. As nearest neighbours of zinc, 4 nitrogen atoms are present in a distance of 1.93 Å (Table 1, part b). The second peak indicates the corresponding carbon atoms of the cyanide group at 3.22 Å. In both EXAFS spectra (Cu and Zn), a metallic neighbour can be fit in a

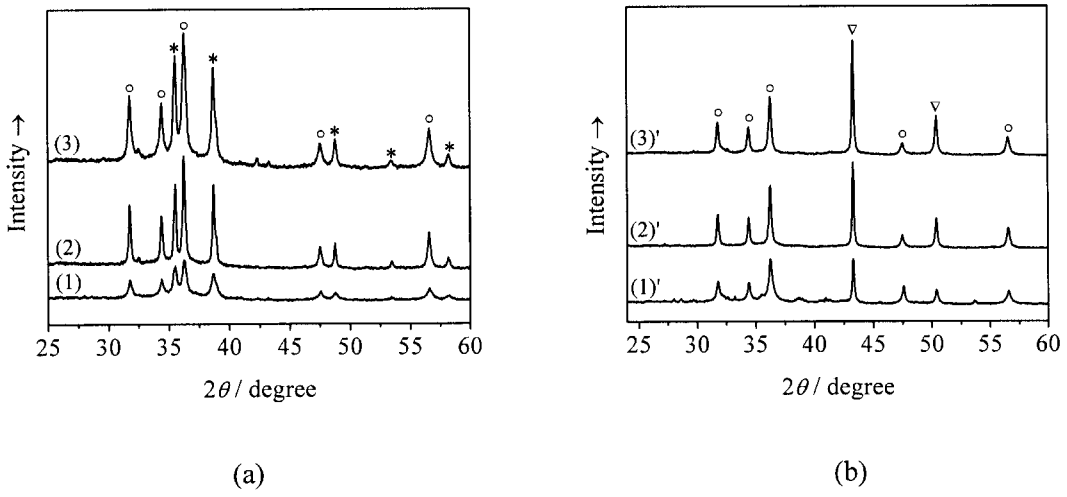

Figure 4. (a) XRD patterns of CuO/ZnO obtained by oxidation of $Zn[Cu(CN)_3]$ at 300 °C (1), 400 °C (2) and 500 °C (3) for 3 hours; (b) XRD patterns of Cu/ZnO obtained by reduction of the corresponding oxide mixtures under H_2/N_2 for 3 hours at 250 °C. The marked peaks correspond to ZnO (o), CuO (*) and Cu (∇).

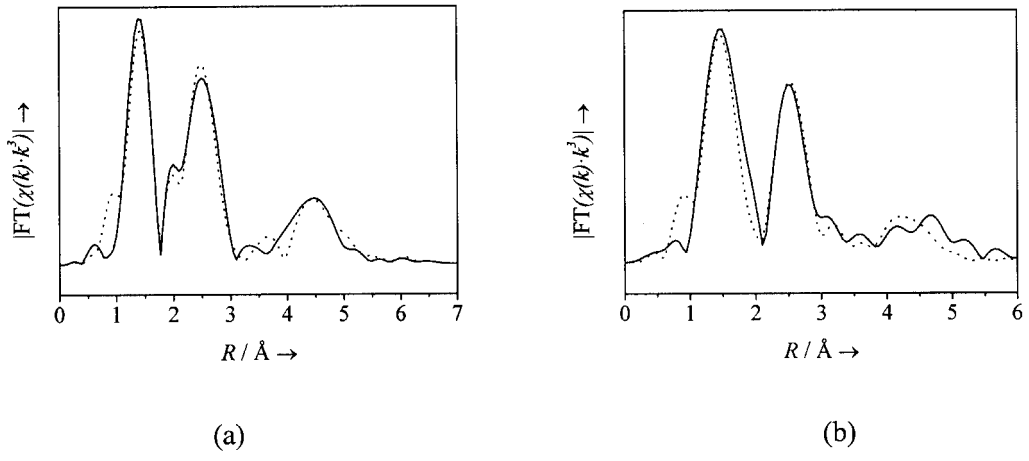

Figure 5. EXAFS Fourier transform magnitudes of the $Zn[Cu(CN)_3]$ prepared by the batch precipitation method. Solid line: experimental data, dot line: fit data. Cu *K*-edge (a) and Zn *K*-edge (b).

distance of 5.1 to 5.2 Å. By EXAFS, we cannot distinguish between a copper neighbour and a zinc neighbour, but the given stoichiometry suggests a network which consists of Cu–C–N–Zn units that connect fourfold-coordinated Cu and Zn centres.

Table 1. Fit parameters for the Cu *K*-edge (a) and Zn *K*-edge (b) EXAFS spectra of $Zn[Cu(CN)_3]$ prepared by the batch precipitation method.

(a) $Zn[Cu(CN)_3]$	*R* [Å]	Coordination number	$\sigma^2 \cdot 10^3$ [Å^2]
Cu – 3 C	1.92	3.1	3.3
Cu – C	2.37	1.0	2.8
Cu – 3 N	3.12	3.2	0.1
Cu – N	3.71	1.4	4.2
Cu – 4 Zn	5.12	4.2	5.9
(b) $Zn[Cu(CN)_3]$	*R* [Å]	Coordination number	$\sigma^2 \cdot 10^3$ [Å^2]
Zn – 4 N	1.93	4.4	6.6
Zn – 4 C	3.22	4.3	3.0
Zn – 4 Cu	5.20	4.3	5.8

In the Cu *K*-edge FTs of the CuO/ZnO mixture (Figure 6, part a), the shells of Cu–O and Cu–Cu in CuO are clearly present, supporting the X-ray diffraction data (Table 2, part a).[23] Figure 6 (part b) shows the Cu *K*-edge FTs of the reduced samples (Cu/ZnO). The Cu–Cu distances of the first shell are in the range of 2.69–2.74 Å (Table 2, part b), and compare well to that of the bulk metal (2.56 Å). The coordination numbers were about 12, also in agreement with the cubic close packing of the bulk metal. The second shell of copper was at a distance of about 3.5 Å with a coordination number of 6. The weak peaks at about 1.5 Å may result from CuO or Cu_2O (in bulk Cu_2O the first coordination number is 2 and the Cu–O distance is 1.84 Å; see also the results for CuO).[24] Possibly, this is the result of an oxidation of the copper surface due to exposure to air before the EXAFS measurement.

The morphology of the Cu–Zn cyanide complex and the thermolysis products were studied by scanning electron microscopy (Figure 7, parts a–d). The initial complex crystallized as micrometer-scale platelets which were destroyed

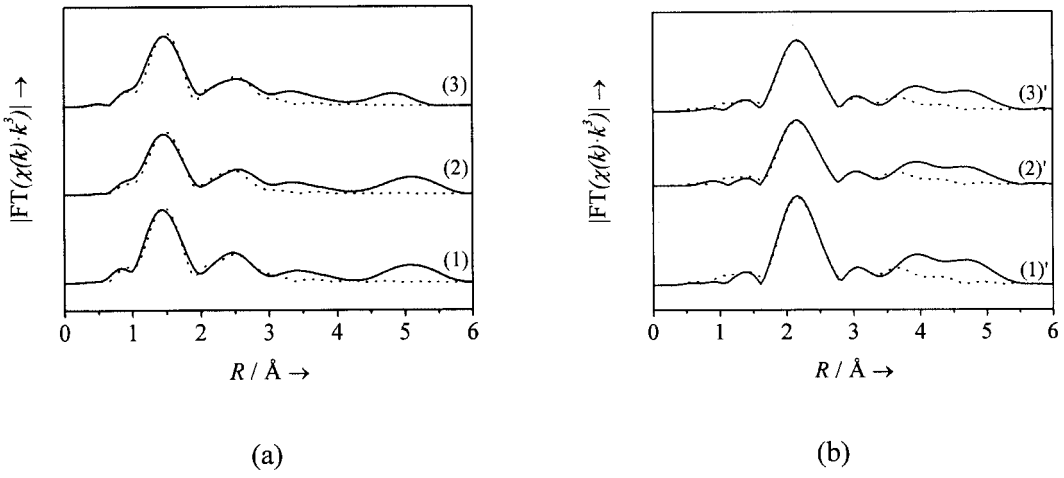

Figure 6. Cu *K*-edge EXAFS Fourier transform magnitudes of (a) CuO/ZnO obtained by thermolysis of $Zn[Cu(CN)_3]$ at 300 °C (1), 400 °C (2) and 500 °C (3) under air for 3 h; (b) Cu/ZnO reduced from the above-mentioned thermolysis products under H_2/N_2 at 250 °C for 3 h. Solid line: experimental data, dot line: fit data.

Table 2. Fit parameters for the Cu *K*-edge EXAFS spectra of CuO/ZnO obtained by thermolysis of $Zn[Cu(CN)_3]$ at 300 °C, 400 °C and 500 °C under air for 3 h (a); and Cu/ZnO reduced from the corresponding thermolysis products under H_2/N_2 at 250 °C for 3 h (b).

(a) CuO/ZnO	Cu – 4 O *R* [Å]	Coordination number	$\sigma^2 \cdot 10^3$ [Å]^2	Cu – 8 Cu *R* [Å]	Coordination number	$\sigma^2 \cdot 10^3$ [Å^2]
300 °C	1.94	3.9	5.5	2.91	8.4	19.9
400 °C	1.96	3.9	4.0	2.93	8.2	22.9
500 °C	1.96	3.8	5.5	2.94	8.1	23.2
(b) Cu/ZnO	Cu – 12 Cu *R* [Å]	Coordination number	$\sigma^2 \cdot 10^3$ [Å]^2	Cu – 6 Cu *R* [Å]	Coordination number	$\sigma^2 \cdot 10^3$ [Å^2]
300 °C/250 °C	2.74	11.9	6.5	3.48	6.8	17.9
400 °C/250 °C	2.69	11.9	7.1	3.41	6.5	13.0
500 °C/250 °C	2.74	12.2	6.9	3.49	6.6	17.1

by the following thermolysis. The diameter of the agglomerates decreased at higher thermolysis temperatures, in contrast to the crystallite size determined by XRD, which increased with increasing temperatures. However, the macroscopic morphology is not directly related to the internal domain size.

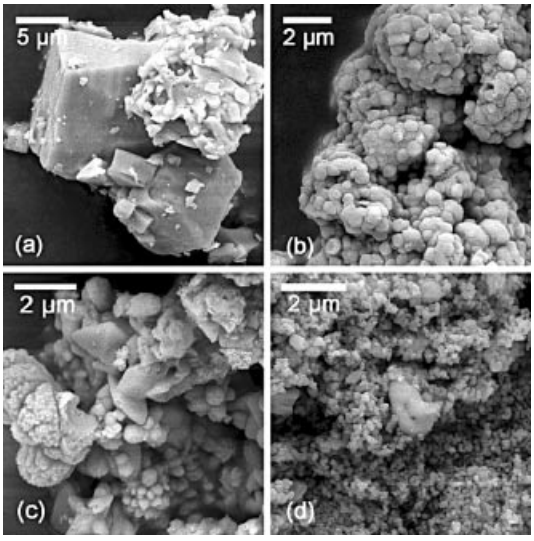

Figure 7. SEM images of $Zn[Cu(CN)_3]$ from batch preparation (a) and its thermolysis products (CuO/ZnO) obtained under air for 3 h at 300 °C (b), 400 °C (c), 500 °C (d), respectively.

Continuous Overflow Preparation

In the continuous overflow precipitation method, the properties of the product can be better controlled in comparison to the simple batch-wise crystallisation. Main variation parameters are the residence time and the concentrations.

We studied the morphology of the Cu–Zn cyanide complex as a function of the solution concentration and the average residence time (related to the flow rate), respectively. First, the concentration was varied at a constant flow rate. It can be seen in Figure 8 parts a–c) that with increasing concentrations of Cu^{2+} and $[Zn(CN)_4]^{2-}$, the complex morphology changed from platelets to spherical particles and the size decreased. Second, the residence time was varied at a constant concentration. This effect is obvious (Figure 8, parts d–f): A shorter residence time led to smaller particles. Hence, we can conclude that higher concentration and low residence time (or high flow rate) both lead to smaller spherical (nano-)particles instead of well-crystalline microcrystals (platelets). Elemental analysis of the sample in Figure 8 (part f) gave a Cu/Zn/CN ratio of 1:1:3.04 (16.8 wt.-% C, 19.6 wt.-% N, 29.0 wt.-% Cu, and 30.6 wt.-% Zn), which indicates that $Zn[Cu(CN)_3]$ was still the main component of the precipitates obtained by continuous overflow method, even at the highest concentration and the shortest residence time.

Conclusions

In summary, a batch-wise and a continuous synthesis method were applied to the precipitation of the copper–zinc coordination compound $Zn[Cu(CN)_3]$. Structurally, this compound consists of Cu–C–N–Zn units that bridge Cu and Zn centres (both in fourfold coordination). With the continuous overflow precipitation method, fine spherical particles are obtained at high solution concentration and short residence time (or a high flow rate). The thermolysis of the cyanides was studied in-situ by TG-IR and TG-MS. Under oxidizing conditions, cyanogen is lost only at lower temperature whereas at higher temperature, thermal decomposition to carbon and nitrogen oxides occurs. The product is a 1:1 mixture of CuO and ZnO which can be reduced to Cu/ZnO, a well-known catalyst.

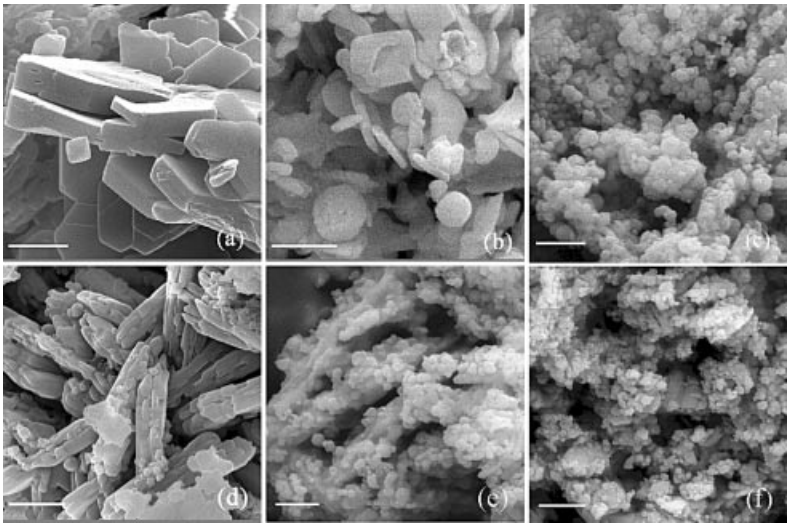

Figure 8. SEM images of $Zn[Cu(CN)_3]$ prepared by continuous overflow method with different $[Zn(CN)_4]^{2-}$ concentrations (residence time of 30 s), i.e., 0.05 mol L^{-1} (a), 0.3 mol L^{-1} (b), 0.4 mol L^{-1} (c) and different residence time (constant concentration of 0.4 mol L^{-1}), i.e., 140 s (d), 30 s (e), 15 s (f). Cu^{2+} and $[Zn(CN)_4]^{2-}$ were always present in stoichiometric ratios (1:1). Scale bar: 1 µm.

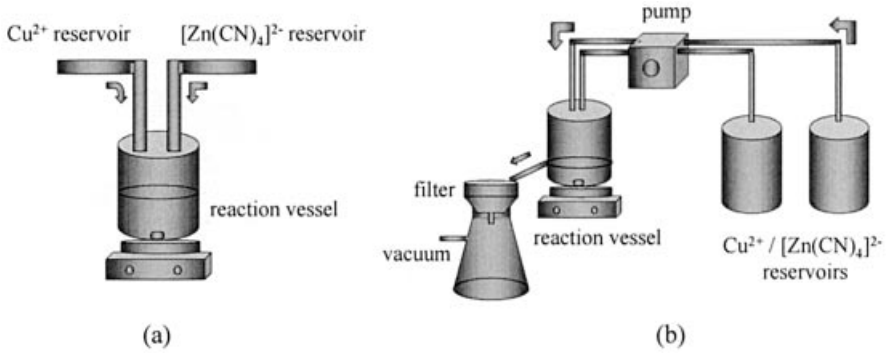

Figure 9. Schematic setups of the batch precipitation method (a) and the continuous overflow method (b).

Experimental Section

In the batch precipitation method (Figure 9, part a), $[Zn(CN)_4]^{2-}$ was prepared by mixing aqueous solutions of zinc sulfate and potassium cyanide. Copper(II) sulfate was then added whilst stirring and copper zinc cyanide was obtained as precipitate. In the continuous overflow precipitation method (Figure 9, part b), the aqueous solutions of $K_2[Zn(CN)_4]$ and $CuSO_4$ were pumped at different flow rates (giving different residence time) into a stirred precipitation vessel at room temperature. The overflowing suspension was immediately filtered. The precipitate was dried overnight under air at room temperature and stored in sealed vials until further characterization. All reagents were used in stoichiometric amounts, i.e. $n(Cu) = n(Zn)$.

The controlled thermolysis of the cyanides was carried out in a horizontal quartz tube reactor with an inner diameter of 30 mm. The thermal decomposition was carried out under air at 300, 400 and 500 °C for 3 hours. The mixed oxides were then reduced under hydrogen/nitrogen (5:95, *v*:*v*) at 250 °C for 3 hours.

Combined thermogravimetry-infrared spectroscopy (TG-IR) was carried out with a Netzsch STA 409 TG-DTA/DSC apparatus connected to a Bruker Vertex 70 infrared system for in-situ gas analysis. Samples were heated from room temperature to 1000 °C at a rate of 5 K min^{-1} under O_2 at a flow rate of 50 mL min^{-1}. The evolved gases were monitored in-situ by infrared spectroscopy (IR). The infrared spectra were all corrected for background absorption. Background spectra were recorded at room temperature before the start of the experiment with the cavity filled by flow gas. Thermogravimetry-mass spectroscopy (TG-MS) was carried out with a TGA 7 Perkin–Elmer thermobalance coupled to a quadrupole mass spectrometer (OmniStar™, Pfeiffer). The sample was heated up with 10 K min^{-1} under synthetic air (20.5% oxygen in nitrogen) at a flow rate of 100 mL min^{-1}.

X-ray diffraction was carried out at room temperature at beamline B2 at the Hamburger Synchrotronstrahlungslabor (HASYLAB) at Deutsches Elektronen Synchrotron (DESY), Hamburg, Germany.

The morphology of the thermolysis products was studied by scanning electron microscopy (LEO Gemini 1530). Extended X-ray absorption fine structure (EXAFS) spectroscopy was carried out at beamline E4 at HASYLAB/DESY. The programs SPLINE and XFIT[25] were used for quantitative data evaluation. Theoretical standards were computed with the program FEFF 6.01a.[26] The amplitude reduction factor S_o^2 was fixed to 1. Variation parameters were the bond lengths, the coordination numbers, the Debye-Waller factors (σ^2), and the zero-energy correction (E_o).

Acknowledgments

This work was supported by the Deutsche Forschungsgemeinschaft within the scope of the Collaborative Research Center SFB 558: Metal–substrate interactions in heterogeneous catalysis. We are grateful for Prof. M. Muhler for TG-MS measurements. We thank J. Gering for experimental assistance. Synchrotron beamtime by HASYLAB at DESY was generously provided.

[1] O. Vazquez Cuchillo, U. Pal, C. Vazquez Lopez, *Modern Phys. Lett. B* **2001**, *15*, 675–678.
[2] S. M. Zhou, X. H. Zhang, X. M. Meng, K. Zou, X. Fan, S. K. Wu, S. T. Lee, *Nanotechnology* **2004**, *15*, 1152–1155.
[3] L. Guo, S. Yang, *Chem. Mater.* **2000**, *12*, 2268–2274.
[4] A. M. Pollard, M. S. Spencer, R. G. Thomas, P. A. Williams, J. Holt, J. R. Jennings, *Appl. Catal. A* **1992**, *85*, 1–11.
[5] Y. Choi, K. Futagami, F. Fijitani, J. Nakamura, *Appl. Catal. A* **2001**, *208*, 163–167.
[6] K. D. Jung, O. S. Joo, *Catal. Lett.* **2002**, *84*, 21–25.
[7] H. Wilmer, T. Genger, O. Hinrichsen, *J. Catal.* **2003**, *215*, 188–198.
[8] R. Naumann d′Alnoncourt, M. Kurtz, H. Wilmer, E. Loeffler, V. Hagen, J. Shen, M. Muhler, *J. Catal.* **2003**, *220*, 249–253.
[9] B. L. Kniep, T. Ressler, A. Rabis, F. Girgsdies, M. Baenitz, F. Steglich, R. Schlögl, *Angew. Chem.* **2004**, *116*, 114–117; *Angew. Chem. Int. Ed.* **2004**, *43*, 112–115.
[10] M. Kurtz, H. Wilmer, T. Genger, O. Hinrichsen, M. Muhler, *Catal. Lett.* **2003**, *86*, 77–80.
[11] J. Hambrock, M. K. Schroeter, A. Birkner, C. Woell, R. A. Fischer, *Chem. Mater.* **2003**, *15*, 4217–4222.
[12] M. Rehbein, M. Epple, R. D. Fischer, *Solid State Sci.* **2000**, *2*, 473–488.
[13] M. Rehbein, R. D. Fischer, M. Epple, *Thermochim. Acta* **2002**, *382*, 143–149.
[14] Y. Guo, R. Weiss, M. Epple, *J. Mater. Chem.* **2005**, *15*, 424–429.
[15] T. Welzel, W. Meyer-Zaika, M. Epple, *Chem. Commun.* **2004**, 1204–1205.
[16] M. M. Günter, T. Ressler, B. Bems, C. Büscher, T. Genger, O. Hinrichsen, M. Muhler, R. Schlögl, *Catal. Lett.* **2001**, *71*, 37–44.
[17] B. Bems, M. Schur, A. Dassenoy, H. Junkes, D. Herein, R. Schlögl, *Chem. Eur. J.* **2003**, *9*, 2039–2052.
[18] M. Schur, B. Bems, A. Dassenoy, I. Kassatkine, J. Urban, H. Wilmes, O. Hinrichsen, M. Muhler, R. Schlögl, *Angew. Chem.* **2003**, *115*, 3945–3947; *Angew. Chem. Int. Ed.* **2003**, *42*, 3815–3817.
[19] R. M. Izatt, J. J. Christensen, J. W. Hansen, G. D. Watt, *Inorg. Chem.* **1965**, *4*, 718–721.
[20] R. Paterson, J. Bjerrum, *Acta Chim. Scand.* **1965**, *19*, 729–734.

[21] J. Cernak, Z. Zak, J. Chomic, C. Kappenstein, *Acta Crystallogr. C* **1998**, *54*, 1551–1553.
[22] A. G. Sharpe, *The Chemistry of cyano complexes of the transition metals*, Academic Press, London, **1976**.
[23] W. Grünert, N. W. Hayes, R. W. Joyner, E. S. Shapiro, M. R. H. Siddiqui, G. N. Baeva, *J. Phys. Chem. A* **1994**, *98*, 10832–10846.
[24] G. U. Kulkarni, C. N. R. Rao, *Top. Catal.* **2003**, *22*, 183–189.
[25] P. J. Ellis, H. C. Freeman, *J. Synchrotron Radiat.* **1995**, *2*, 190–195.
[26] E. A. Stern, M. Newville, B. Ravel, Y. Yacoby, D. Haskel, *Physica B* **1995**, *208–209*, 117–120.

Received: February 2, 2005
Published Online: June 22, 2005

